Modeling and Simulation of an Industrial Ethylene Oxide (EO) Reactor Using Artificial Neural Networks (ANN)

ARTICLE *in* INDUSTRIAL & ENGINEERING CHEMISTRY RESEARCH · APRIL 2011

Impact Factor: 2.59 · DOI: 10.1021/ie101319d

3 AUTHORS, INCLUDING:

M. R. Rahimpour
Shiraz University
331 PUBLICATIONS **3,005** CITATIONS

SEE PROFILE

I&EC research
Industrial & Engineering Chemistry Research

ARTICLE

pubs.acs.org/IECR

Modeling and Simulation of an Industrial Ethylene Oxide (EO) Reactor Using Artificial Neural Networks (ANN)

M. R. Rahimpour,*,† M. Shayanmehr,† and M. Nazari‡

†Department of Chemical Engineering, School of Chemical and Petroleum Engineering, Shiraz University, Shiraz 71345, Iran
‡Department of Chemical Engineering, Amirkabir University of Technology, No. 424, Hafez Ave., Tehran, Iran

ABSTRACT: In the present work, a one-dimensional heterogeneous model was used for dynamic simulation of an industrial fixed-bed catalytic ethylene oxide (EO) reactor in the presence of long-term catalyst deactivation. In order to determine the level of optimum ethylene dichloride (EDC), a multilayer perceptron (MLP) neural network was used. In addition, the effect of inlet gas velocity on EO mole fraction of gas and solid phases was investigated. The model validation was carried out by comparison of model results with corresponding industrial conditions and over a period of three operating years. A good agreement was found between the simulation results of the dynamic model and historical process data. The error of simulation was found to be less than 5%. The results of the artificial neural network (ANN) modeling showed that the maximum selectivity occurs in the range of 0.37−0.42 ppm of EDC. Also, it was observed that with decrease of gas velocity the difference between the EO mole fraction of gas phase and solid phase increases. This behavior was attributed to the distinct resistances of kinetically controlled and the mass transfer resistance of gas film around the catalyst pellets.

1. INTRODUCTION

Ethylene oxide is an important starting chemical in several petrochemical processes which is used for the manufacturing of many useful petrochemicals, such as ethylene glycol (the primary ingredient in antifreezers), poly ethylene oxide, glycol ethers, ethanol amines, surfactants, lubricants, plasticizers, etc.[1,2] The most widely used commercial process to manufacture ethylene oxide is the direct catalytic oxidation of ethylene with air or oxygen over supported silver catalysts with sufficient activity and selectivity in fixed-bed reactors (FBR).[3,4] The main reactions included in the ethylene oxidation process are as follows:[5,6]

$$C_2H_4 + 0.5O_2 \xrightarrow{Ag} C_2H_4O \quad \Delta H_{298} = -105.39\ \frac{kj}{mol} \quad (1)$$

$$C_2H_4 + 3O_2 \xrightarrow{Ag} 2CO_2 + 2H_2O$$
$$\Delta H_{298} = -1321.73\ \frac{kj}{mol} \quad (2)$$

The main stage of the ethylene oxide process is ethylene oxidation reaction (reaction 1) which occurs simultaneously with the reaction 2. The mechanism of these reactions has been reported by Van Santen.[7] Boskovic et al.[8] investigated the deactivation of catalytic system (namely, supported Ag catalysts) through an accelerated approach upon ethylene epoxidation process in a Berty reactor. As an exemplary process, ethylene epoxidation has also been served as the reaction system for modeling and nonlinear behavior studies. The extreme complexity of the processes involved in the ethylene oxide production justify the computer simulation of such processes in order to get further understanding of the system without the need for conducting costly and time-consuming experiments.

From a theoretical viewpoint, in the field of modeling and simulation of catalytic fixed-bed reactors under realistic operating conditions, two different policies have been applied: (1) conventional steady state simulation and (2) dynamic (transient) simulation. The dynamic simulation of ethylene oxidation reactor processes, in particular, has a wide range of applications including; the start-up and shut-down investigations, system identification, safety, control, optimization, and transient behavior and operability studies. In transient conditions, the combination of the dynamic properties of the catalyst, at a microscale level and the dynamic properties of the reactor, at a macroscale level, make it possible to obtain more favorable concentration and temperature profiles for the catalytic process.[9−11] The dynamic simulation is preferred to steady-state simulations in operability studies since the former provides a realistic description of the transient states of the reactor owing to the fact that the numerical solution strategies employed in dynamic models are more robust than the solution of a typical steady-state model.

Some investigations have been performed on simulation of fixed bed reactors. Zhou et al.[2] optimized an industrial ethylene epoxidation process in terms of feed composition, feeding rate and operating pressure using a one-dimensional homogeneous model under steady-state conditions. Hwang et al.[12,13] simulated ethylene oxide reactor with the aim of finding an optimum operating temperature for this reactor under steady-state conditions without taking catalyst deactivation into account. In the work of Cornelio[14] a dynamic heterogeneous model of an industrial EO reactor was developed and then simplified into

Received: June 20, 2010
Accepted: April 1, 2011
Revised: November 18, 2010
Published: April 15, 2011

dx.doi.org/10.1021/ie101319d | *Ind. Eng. Chem. Res.* 2011, 50, 6044–6052

a pseudohomogeneous model. Aryana et al.[15] modeled and optimized an industrial ethylene oxide oil-coolant reactor. They ignored the mass balance on catalyst for species. Sandip Kumar Lahiri et al.[16] used an integrating support vector regression and genetic algorithm to model and optimize an industrial ethylene oxide reactor. Rezaie et al.[17] compared results of the heterogeneous model with the homogeneous model through a dynamic simulation in the presence of catalyst deactivation. Rahimpour et al.[18] studied catalyst deactivation of methanol synthesis results in a deactivation model. Rahimpour et al.[19,20] presented strategies to enhance the ability of methanol synthesis reactor using a mixture of fresh and partially deactivated catalyst. Velardi and Barresi[21,22] proposed a multistage methanol reactor network with autothermal behavior to promote the reactor performance.

In the ethylene oxide reactors, organohalide inhibitors such as ethylene dichloride (EDC) are added (in concentrations less than 1 ppm) to control the reaction rate and improve the selectivity of the catalyst. The complete oxidation of ethylene is inhibited to a great extent by EDC than partial oxidation; hence the selectivity for ethylene oxide is promoted. Therefore, the level of EDC significantly affects the performance of the reactor and its determination is a challenging task for industry. In the above studies experimental equations has been used to estimate the level of EDC. In this consideration, artificial neural network (ANN) can be used as a powerful technique.

Artificial neural networks may be defined as structures comprised of densely interconnected adaptive simple processing elements (artificial neurons) that are capable of performing massively parallel computations for data processing and knowledge representation. The attractiveness of ANNs comes from the remarkable information processing characteristics of the biological system such as nonlinearity, high parallelism, robustness, fault and failure tolerance, learning, ability to handle imprecise and fuzzy information, and their capability to generalize. These characteristics of artificial neural networks are desirable because (i) nonlinearity allows better fit to the data, (ii) high parallelism implies fast processing, (iii) learning and adaptivity allow the system to update (modify) its internal structure in response to changing environment, and (iv) generalization enables application of the model to unlearned data.

Artificial neural network can statistically model nonlinear function relationships through a network of nodes or neurons. The nodes are connected together by weighted links. The weights are adjusted through training algorithm and examples. Among the various kinds of existing ANN approaches, the multilayer perceptron (MLP) neural networks have become the most popular in engineering applications.

This paper was aimed to investigate the behavior of an industrial ethylene oxide catalytic reactor using an appropriate mathematical model. A heterogeneous one-dimensional transient model was developed in the presence of long-term deactivation of Ag/Al_2O_3 as catalytic system, considering two different solid and fluid phases along with their corresponding heat and mass exchanges. In order to determine the level of optimum EDC a MLP neural network was used. In addition, the effect of inlet gas velocity on the similarity of gas and solid phase profiles was investigated. Authors believe that the obtained results can be used to improve the performance of industrial reactors.

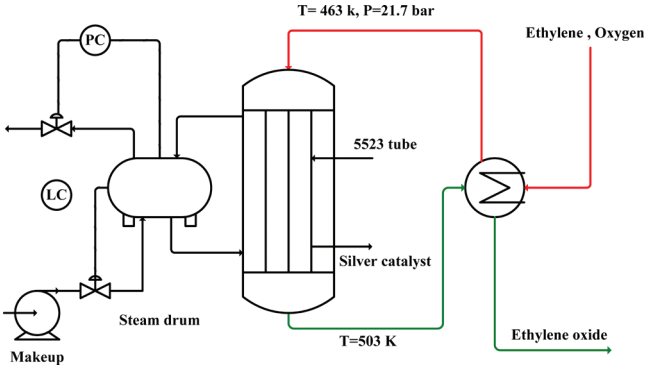

Figure 1. Process flow diagram of an ethylene oxide reactor.

Table 1. Ethylene Oxide Reactor Feed Inlet Condition[23]

quantity	value
C_2H_4 (mole %)	25.00
O_2 (mole %)	8.00
CO_2	7.00
H_2O	0.25
C_2H_4O	0.01
CH_4	47.03
N_2	12.71
total molar flow rate per tube (mol/s)	0.89
inlet temperature (K)	463
inlet pressure (bar)	21.7
coolant temperature (K)	503
balance gas	methane

2. PROCESS DESCRIPTION

The process flow diagram (PFD) of a conventional ethylene oxide reactor is shown in Figure 1. Such a reactor usually resembles a vertical shell and tube heat exchanger. The tubes are packed with Ag catalyst pellets and boiling water is circulating in the shell side to remove the heat of exothermic reactions and to provide fixed temperature around the tubes of reactor. The reactor temperature is controlled by controlling vapor pressure of the boiling water. Also chloride components (ethylene dichloride (EDC)) are added into the reactor to increase selectivity. The coolant temperature is varied with time in order to cope with a decrement in ethylene oxide yield because of catalyst deactivation.

In the current work, the feed flow rate, feed compositions and also catalyst and reactor specifications have been collected from reference[23] as a case study and are tabulated in Tables 1 and 2, respectively.

3. MODEL DEVELOPMENT

3.1. Mathematical Model. In this study, a heterogeneous one-dimensional model, which is a conventional model for a catalytic reactor with heat and mass transfer resistances,[17] has been developed in order to determine the concentration and temperature distributions inside the reactor.[24,25] Also, the gradient between solid and fluid phases is considered. In industrial tubular reactors, axial dispersion can be neglected because of the comparatively small radius of the tube and a high gas velocity. Further, the catalytic system is assumed as isothermal pellets

Table 2. Catalyst and Reactor Specifications

quantity	value
ρ_s (kg/m^3)	890
d_p (m)	7.74×10^{-3}
C_{ps} (j/kg K)	1000
void fraction	0.5
a_v (m^2 m^{-3})	387.59
number of tubes	5523
length of reactor (m)	8.7
tube diameter (m)	private

Table 3. Molecular Weight and Critical Volume of the Components

component	M_i (g/mol)	$v_{ci} \times 10^6$ (mol/m^3)
C_2H_4	28.054	129.1
O_2	32.00	73.4
C_2H_4O	44.054	140.3
CO_2	44.01	94
H_2O	18.01	56
CH_4	16.04	99.0
N_2	28.01	18.5

along the reactor length. The balances typically account for accumulation, convection, and transport to the solid-phase, where the resulted conservation equations coupled through thermodynamic and kinetic relations, as well as, auxiliary correlations for predicting physical properties.[26]

These conservation equations were derived according to the following assumptions:[22,25,27,28]

- One-dimensional flow is considered.
- Plug flow is employed.
- Axial diffusion of mass and heat is negligible.
- Heat loss to surrounding is neglected.
- Ideal gas behavior is assumed.To obtain the mass and energy balance equations, a differential element along the axial direction inside the reactor was considered. The balances typically account for convection, transport to the solid-phase and reaction.

3.1.1. Solid Phase. The mass and energy balances for the solid phase are expressed by

$$\varepsilon_s c_t \frac{\partial y_{is}}{dt} = K_{g_i}(y_i - y_{is}) + \eta r_i \rho_B a \quad i = 1, 2, \ldots, N-1 \qquad (3)$$

$$\rho_B c_{ps} \frac{\partial T_s}{dt} = a_v h_f (T - T_s) + \rho_B a \sum_{i=1}^{N} \eta r_i (-\Delta H_{f,i}) \qquad (4)$$

In eq 3, y_{is} is the solid-phase mole fraction and C_t is the total concentration. On the right-hand side, K_{g_i} is the mass transfer coefficient for component a is the activity of catalyst, ρ_B is the density of catalytic bed and η is effectiveness factor, which is obtained from dusty gas model calculations. In eq 4, C_{ps}, T_s, a_v, and h_f are the specific heat of the solid at constant pressure, the temperature of solid phase, the specific surface area of catalyst pellet and, the gas−solid heat transfer coefficient, respectively.

Table 4. Components Heat Capacity (T = 487 K)

component	a	b	c	d	C_p
ethylene	32.083	-0.00148	2.47×10^{-4}	-2.40×10^{-7}	66.10
oxygen	29.526	-9.00×10^{-3}	3.80×10^{-5}	-3.26×10^{-8}	30.89
ethylene oxide	30.827	-7.40×10^{-3}	3.20×10^{-4}	-3.30×10^{-7}	70.52
CO_2	27.437	4.23×10^{-2}	-1.90×10^{-5}	4.00×10^{-9}	43.98
H_2O	33.933	-8.40×10^{-3}	3.00×10^{-5}	-1.78×10^{-8}	35.11

Table 5. Deactivation Parameters

k_{d0} (month^{-1})	E_d (kJ mol^{-1})	a_∞
4.00×10^{11}	120	0.3
2.806×10^{7}	80	0.3
2.00×10^{3}	40	0.3

3.1.2. Fluid Phase. The following mass and energy balances equations are written for the fluid phase:

$$\varepsilon_B c_t \frac{\partial y_i}{\partial t} = -\frac{F_t}{A_c}\frac{\partial y_i}{\partial z} + a_v c_t k_{g_i}(y_{is} - y_i) \quad i = 1, 2, \ldots, N-1 \qquad (5)$$

$$\varepsilon_B c_t c_{pg} \frac{\partial T}{\partial t} = -\frac{F_t}{A_c}\frac{\partial T}{\partial z} + a_v h_f (T_s - T) + \frac{\pi D_i}{A_c} U_{shell}(T_{shell} - T) \qquad (6)$$

In eq 5, ε_B and y_i are the void fraction of catalytic bed and the gas-phase mole fraction, respectively. On the right-hand side, F_t and A_c are the total molar flow per tube and the across section area of each tube.

In eq 6, c_{pg}, T_{shell}, and U_{shell} are the specific heat of the gas at constant pressure, the temperature of coolant stream and overall heat transfer coefficient between coolant and process streams, respectively.

3.1.3. Boundary Conditions. At the entrance of the reactor, the inlet temperature, the inlet pressure and the inlet gas compositions of the reactant gas are known. Therefore, the following boundary conditions are applied

$$z = 0; y_i = y_{i0}, T = T_0 \qquad (7)$$

while the initial conditions are

$$t = 0; y_i = y_i^{ss}, y_{is} = y_{is}^{ss}, T = T^{ss}, T_s = T_s^{ss}, a = 1 \qquad (8)$$

where y_i^{ss} and y_{is}^{ss} are the steady state profiles of mole fractions and T^{ss} and T_s^{ss} are the steady state profiles of temperature along the reactor length. The values of T^{ss} and T_s^{ss} are determined from a steady state simulation.

3.2. Auxiliary Equations. To complete the simulation, auxiliary correlations should be added to the model. In the heterogeneous model, because of transfer phenomena, the correlations of estimation of heat and mass transfer between two phases and estimation of physical properties of chemical species and overall heat transfer coefficient between two sides should be considered. The correlations used for physical properties, mass and heat transfer coefficient are summarized in below.

3.2.1. Mass Transfer Coefficients. In current work, mass transfer coefficients for the components have been taken from

dx.doi.org/10.1021/ie101319d |*Ind. Eng. Chem. Res.* 2011, 50, 6044–6052

Table 6. Range of Data Sets Used in This Work

parameter	minimum value	maximum value	standard deviation
EDC (ppm)	0	0.9	0.246
E_d (kJ mol^{-1})	40	120	39.6
ethylene oxide concentration (%)	1.8	2.2	0.165

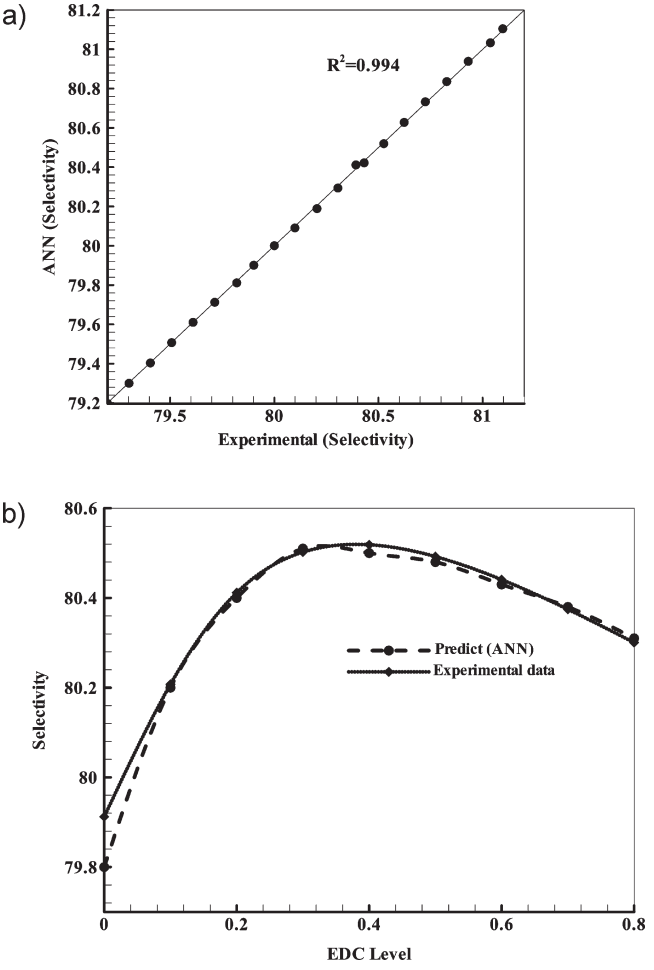

Figure 2. (a) LM algorithm of model trained for testing data set. (b) Comparison of between ANN and experimental data vs EDC level in E_d = 80 kJ mol^{-1} and ethylene oxide concentration(%) = 2.

literature.[29] These are mass transfer coefficients between gas phase and solid phase.

$$k_{gi} = 1.17Re^{-0.42}Sc_i^{-0.67}u_g \times 10^3 \quad (9)$$

where the Reynolds and Schmidt numbers are defined as

$$Re = \frac{2R_p u_g}{\mu} \quad (10)$$

$$Sc_i = \frac{\mu}{\rho_g D^i{}_m \times 10^{-4}} \quad (11)$$

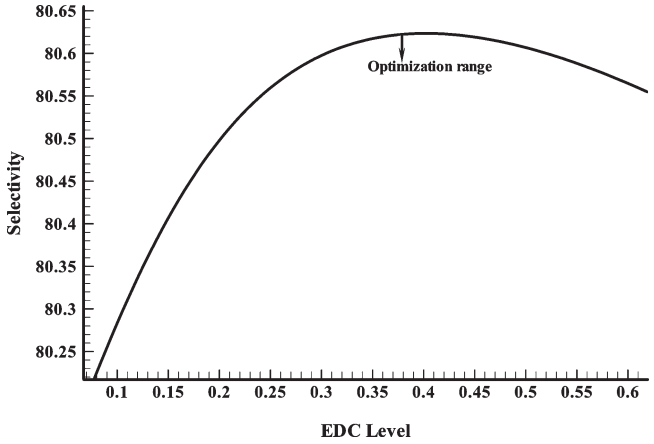

Figure 3. Network outputs for varied input EDC and optimization range.

Diffusivity of component i in the gas mixture ($D_{i,m}$) is given by:[30,31]

$$D_{i,m} = \frac{1 - y_i}{\sum_{i=j} \frac{y_i}{D_{ij}}} \quad (12)$$

Binary diffusivities in eq 12 have been calculated using the Fuller−Schetter−Giddins equation as below[32]

$$D_{ij} = \frac{10^{-7}T^{3/2}\sqrt{\frac{1}{M_i} + \frac{1}{M_j}}}{P\left(v_{ci}{}^{3/2} + v_{cj}{}^{3/2}\right)^2} \quad (13)$$

Values of v_{ci} (critical volume) and M_i (molecular weight) are given in Table 3.

3.2.2. Heat Transfer Correlations. The overall heat transfer coefficient between the boiling water in the shell side and the bulk of the gas phase in the tube side is given by the following correlation:

$$\frac{1}{U_{shell}} = \frac{1}{h_i} + \frac{A_i \ln\left(\frac{D_o}{D_i}\right)}{2\pi L K_w} + \frac{A_i}{A_o}\frac{1}{h_o} \quad (14)$$

where h_i is the heat transfer coefficient between the gas phase and reactor wall and h_o is the heat transfer coefficient of boiling water in the shell side, which are obtained by the following correlations, respectively:[33,34]

$$\frac{h_i}{C_p \rho \mu}\left(\frac{C_p \mu}{K}\right)^{2/3} = \frac{0.458}{\varepsilon_B}\left(\frac{\rho u d_p}{\mu}\right)^{-0.407} \quad (15)$$

$$h_o = 7.96(T - T_{sat})^3\left(\frac{P}{P_a}\right)^{0.4} \quad (16)$$

where u is the superficial velocity of gas and the other parameters are those of bulk gas phase and d_p is the equivalent catalyst diameter, ε_B is void fraction of catalyst bed, K is thermal conductivity of gas, and ρ and μ are density and viscosity of gas, respectively.

The last term of the eq 16 has been considered because of the effect of pressure on the boiling heat transfer coefficient. For the heat transfer coefficient between bulk gas phase and solid phase (h_f), eq 15 has been applied. Components heat capacity has been

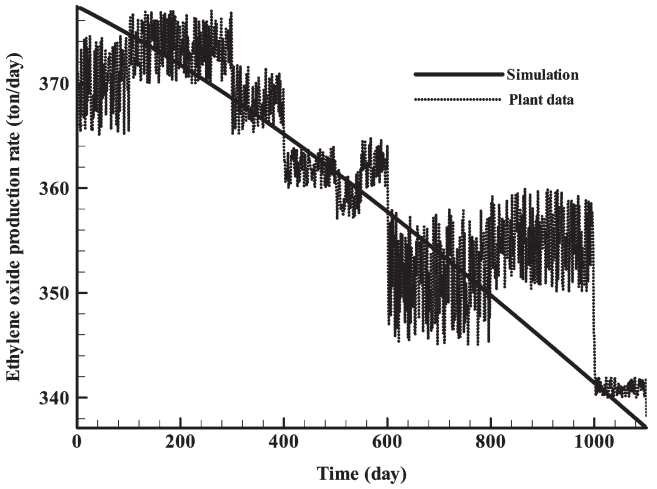

Figure 4. Comparison of plant production rate and estimated production rate by the heterogeneous model.

calculated by a third order polynomial equation with the general form of $C_p = a + bT + cT^2 + dT^3$. The values of constants a, b, c, and d are given in Table 4.

3.3. Reaction Kinetics. The kinetics of ethylene oxidation has been studied extensively by a number of authors[2,5,6 and 35]. In the current work, the rate expressions have been selected from Gu et al.[36]

$$r_{EO} = \frac{\exp\left(\frac{10.30 - 8358.5}{T}\right) P_{ET} {P_{O2}}^{0.75}}{1 + D_n} \quad (17)$$

$$r_{CO_2} = \frac{\exp\left(\frac{12.54 - 9835.2}{T}\right) P_{ET} P_{O_2}}{1 + D_n} \quad (18)$$

where D_n is defined as follows:

$$D_n = 1 + \exp\left(\frac{9812.8}{T} - 21.68\right) P_{CO_2} + \exp\left(\frac{16129.2}{T} - 34.58\right) {P_{CO_2}}^{0.5} P_{H2O} \quad (19)$$

3.4. Catalyst Deactivation. With their unique ability of promoting selectivity against total oxidation of ethylene, supported silver catalysts are extremely important in ethylene oxide (EO) production. Catalyst deactivation has, however, a negative impact on process economy.[8] Despite the wide list of possible causes for deactivation, it is broadly accepted that sintering of silver is the primary reason causing an irreversible loss of catalyst active sites because of silver crystallite growth.[37]

On the basis of these facts, a second-order general power law equation (GPLE) was considered as a deactivation model for the commercial Ag-based EO synthesis catalyst[2]

$$-\frac{da}{dt} = k_{d0} e^{-E_d/RT} (a - a_\infty)^2 \quad (21)$$

Three groups of deactivation parameters for the optimal performance of the reactor changes with deactivation rate are listed in Table 5.[2]

Table 7. Comparison between predicted ethylene oxide production rates by heterogeneous model with plant data.[23]

		heterogeneous model	
time (day)	plant (t/day)	predicted (t/day)	error percent
0	370.00	377.34	1.98
100	370.60	374.60	1.09
200	372.10	371.75	−0.09
300	369.12	368.50	−0.15
400	368.50	365.18	−0.90
500	361.69	361.53	−0.04
600	360.58	357.74	−0.78
700	347.61	353.81	1.70
800	354.74	349.74	−1.40
900	352.39	345.66	−1.90
1000	345.43	341.45	−1.15
1100	347.20	337.15	2.80

3.5. Numerical Simulation. The formulated model composed of 11 partial differential equations with associated boundary conditions has been solved. The algebraic equations in the model incorporate the initial conditions, the reaction rates, the ideal gas assumption, as well as aforementioned correlations for the heat and mass transfer coefficients and the physical properties of fluids.

The mathematical heterogeneous model forms a system of partial differential equations which is solved by a two-step strategy: first, steady-state identification and second, dynamic solution using the results of first step as the appropriate initial conditions. The partial differential equations are discretized with respect to axial direction into 30 nodes. This provides a set of ordinary differential equations (ODEs) for each node. Steady state model was obtained by setting all the time derivatives of original ODEs in each node to zero and considering the activity term of catalyst equal to one (fresh catalyst). The resulted differential algebraic equations (DAEs) are then solved by Gauss−Newton method using MTLAB software.[22,24,25] Through these initial conditions, the system of algebraic partial differential equations of transient model was solved by Rosenbrok method of order two, which is more efficient for such set of stiff equations.[17,38−40]

3.6. ANN Model and Sensitivity Analysis. ANN modeling normally follows these steps: Determination of input/output parameters; data gathering; analysis and preprocessing of the data; training of the neural network; testing of the trained network; and using the trained network for simulation and prediction. Model training includes the choice of architecture, training algorithms and parameters of the network. The performance of an ANN model depends on the data set used for its training and, however, construction of a reliable data set is therefore the first critical step. The selection of property-related parameters, or input parameters, is based on the physical background of how the target property is determined. Omitting the parameters that are not important benefits the development of the model and simplifies further application.

An MLP network generally consists of one input layer, one or more hidden layers and one output layer. The processing units are arranged in layers. Generally, an iterative nonlinear optimization approach using a gradient descent search method is applied

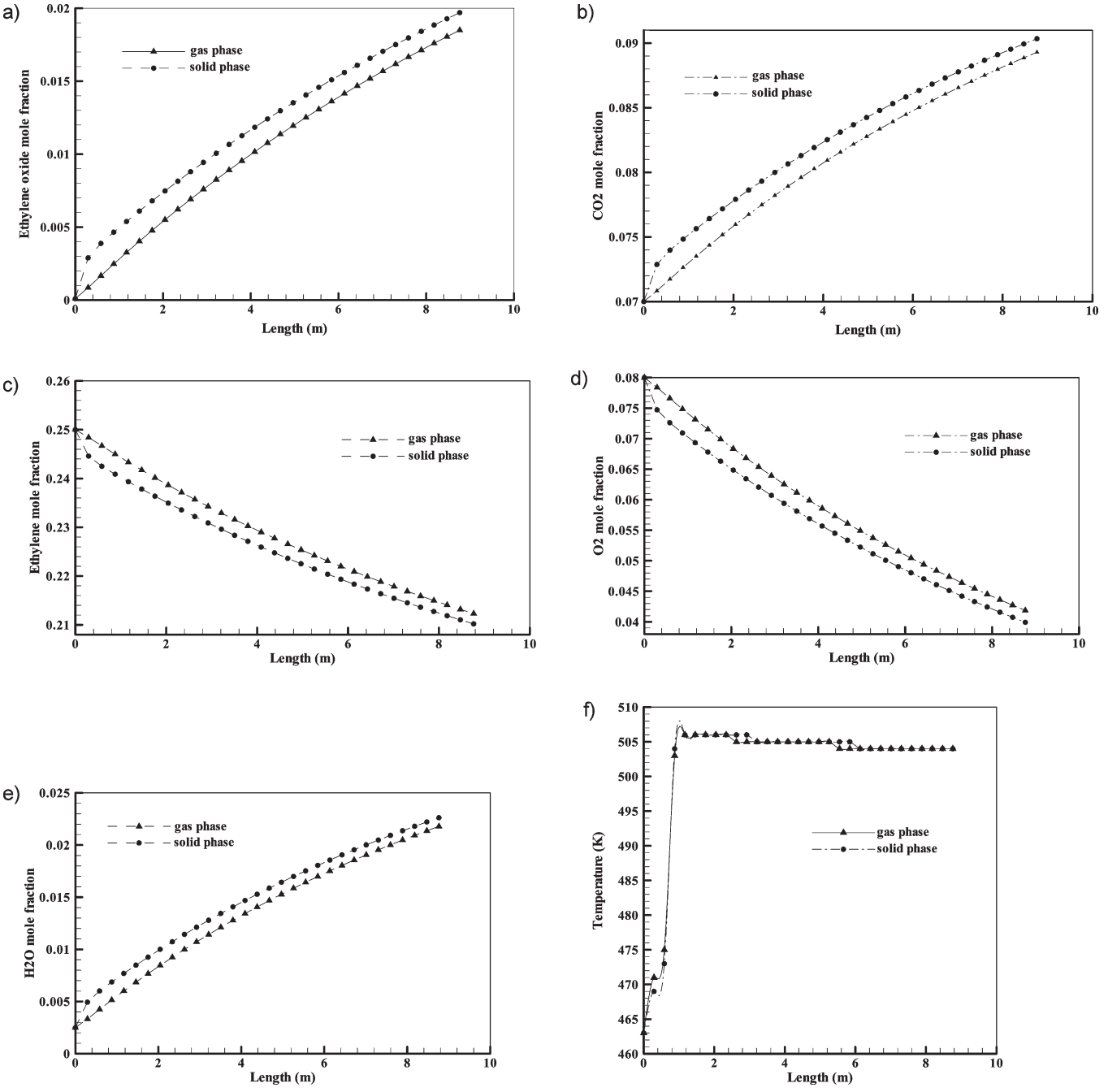

Figure 5. (a) Ethylene oxide mole fraction, (b) CO_2 mole fraction, (c) ethylene mole fraction, (d) O_2 mole fraction, (e) H_2O mole fraction, and (f) temperature profiles along the reactor axis for solid and gas phase under steady-state conditions.

to MLP. It provides a feed forward neural network, giving the capacity to capture and represent relationships between patterns in a given data sample.

In this work, MLP architecture is used for the modeling purpose. The network has three input parameters (EDC, activation energy used in the deactivation model (kJ mol^{-1}) and EO concentration) and one output, which is the value of selectivity. The experimental database used to develop the ANN model has been published by Zhou et al.[2] original references should be consulted for details of testing. It includes 46 data sets of which 34 data sets are used for training (model building) the network and the remaining 12 data sets are selected randomly to test the performance of trained network. The range of data sets is given in Table 6.

Figure 2a represents the performance of the model trained by Levenberg−Marquardt algorithm for the test of data set. In Figure 2a, it is readily observed that the regression coefficient (R^2) of the horizontal axis (experimental data) − the vertical axis (ANN) plot is 0.994 (R^2 = 0.994), which suggests the high correlation between the ANN prediction and the experimental data.

The corresponding values of obtained minimum, maximum errors are 0.0011 and 0.014, respectively. It is observed the model values fit the experimental value well. As shown in Figure.2b, this is in good agreement with the experimental results.[2]

dx.doi.org/10.1021/ie101319d |*Ind. Eng. Chem. Res.* 2011, 50, 6044–6052

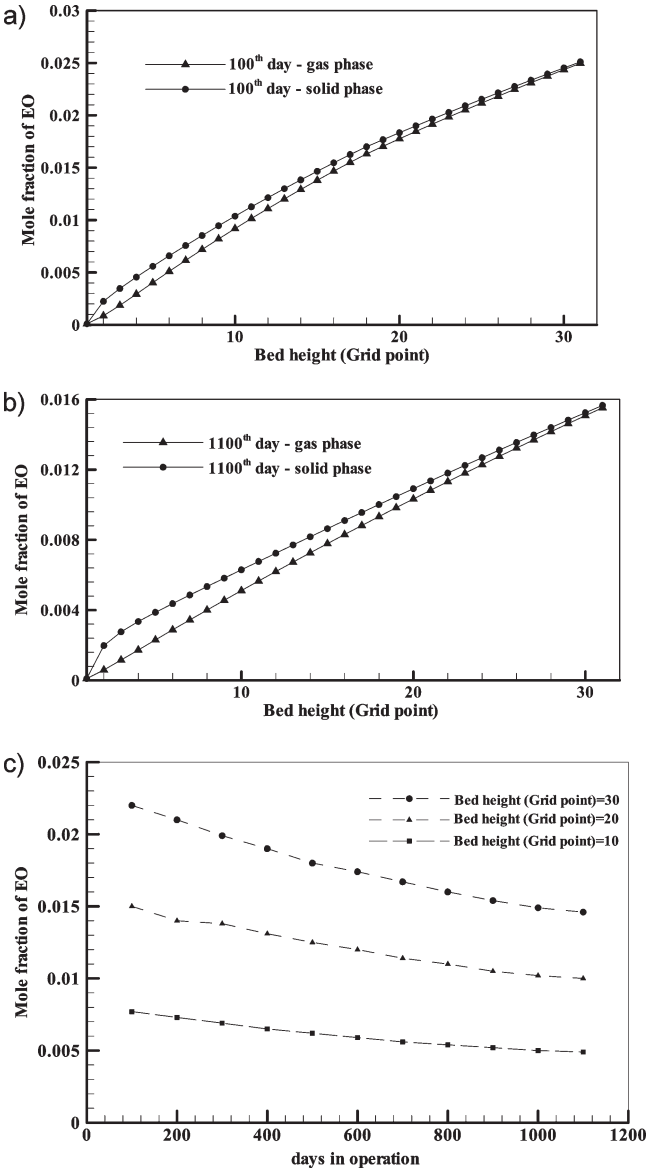

Figure 6. Ethylene oxide concentration profile along the reactor bed for solid and gas phase and after (a) 100 and (b) 1100 operating days. (c) Ethylene oxide concentration profile against operating days at certain grid points, 10, 20, and 30 for gas phase.

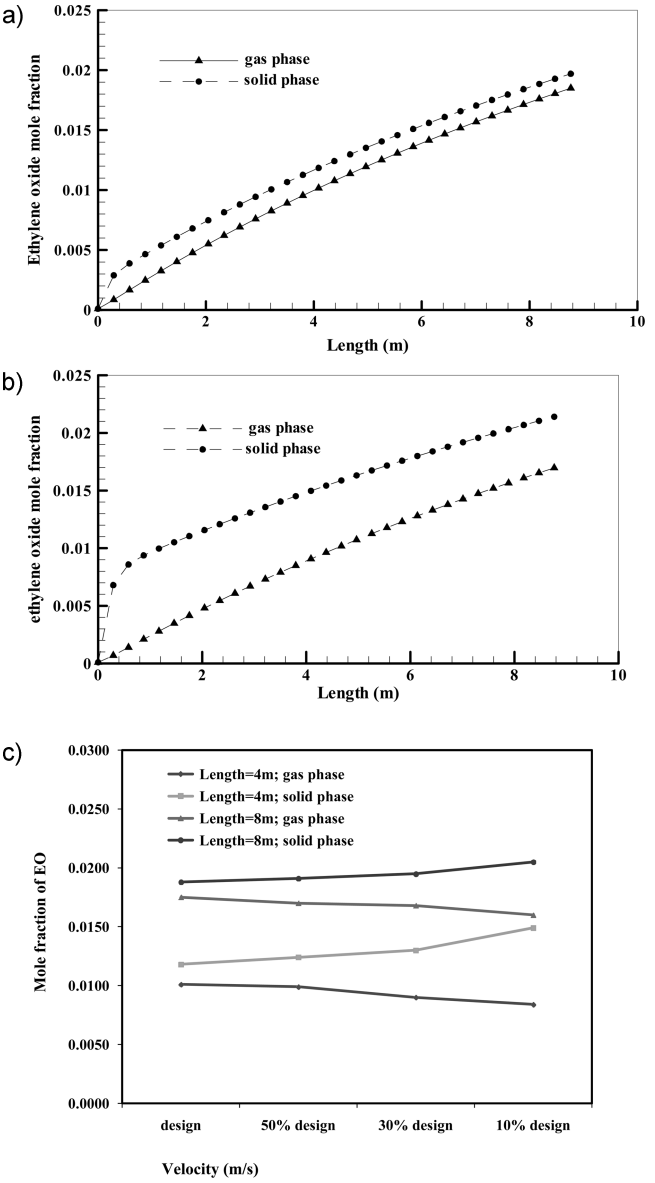

Figure 7. Mole fraction of ethylene oxide along the reactor for different feed linear velocities of (a) design velocity and (b) 10% design velocity. (c) EO mole fraction against the feed linear velocity at certain lengths, 4 and 8 m, for solid and gas phases.

A sensitivity analysis was carried out on the trained neural network to find out the relative importance of processing parameters. In Figure 3, it is readily observed that the maximum of selectivity occurs in the range of 0.37−0.42 ppm of EDC.

4. RESULTS AND DISCUSSION

To verify the performance of heterogeneous dynamic model, simulation results of the model were compared to corresponding historical process data of the plant over a period of about three operating years. Ethylene oxide (EO) production rate (ton/day) was selected as a basis for comparison. In Figure 4, the predicted production rate of EO is compared with that of the plant data. One can see from Figure 4 that the performance of the developed heterogeneous model is acceptable under industrial conditions and a good agreement between simulation results and plant data exists. The maximum bias error of the simulation was less than 3% (Table 7).

This systematic deviation from plant data can be due to the selected ethylene oxidation reaction kinetics which probably underestimates real reaction rates of involved components. Also, the system overhaul/shutdown or accuracy of the experimental data and *etc.* can contribute to the observed discrepancy between the experimental data and the simulated data [17].

Figure 5−e depict the mole fraction profiles of EO, CO_2, C_2H_4, O_2, and H_2O, respectively, under steady state conditions. It can be seen that the predicted values for solid and gas phases change along the reactor axis with a similar trend but different values. The temperature profile of solid and gas phase is presented in Figure 5(f). At the entrance of the reactor, temperature increases sharply which lead to form a hot spot at 507 K. This trend is interrupted by a steadily decreasing trend after 507 K.

One of the important key issues in ethylene oxide reactor configuration is implementing a higher temperature at first parts of

reactor for higher kinetics constants and then gradually reducing the temperature at the end parts of reactor.[22,40−44] The observed difference in the behavior of solid and gas phases can be due to the mass transfer resistance of gas film around the catalyst pellets which affects the transport phenomena between the two phases. Increasing the inlet linear velocity of feed stream can be considered as a practical approach to overcome this problem. In other words, it is believed that high flow rate of reacting material over the catalytic bed results in vanishing mass and heat transfer resistances of gas−solid catalytic reactions.[17] In Figure 5f, there is a maximum in the temperature profile which is due to formation of hot spots. The high rate of the ethylene oxide reaction in the upper section of reactor along with its high exothermicity, especially the heat released by the parallel combustion reaction (eq 2), can be the main reason for this behavior.[6]

In Figure 6, simulation results of heterogeneous model for EO mole fractions in the solid and gas phases have been shown under transient conditions. It is clear that as times goes on, the concentration profiles of both phases approaches to each other and the existing difference between two phases become smaller. It seems that with the decrease in catalyst activity, which is mainly due to thermal sintering, the effect of catalytic system on the external and internal particle mass transfer processes decreases, respectively. So the phases show almost identical results.

It is well accepted that in industrial reactors the higher linear velocity of reactant stream causes close behaviors in the gas and solid phases. Accordingly, ethylene oxide reactor was simulated with different inlet linear velocities of feed stream. Figure 7 shows the effect of velocity of reactant stream on the variation of EO mole fraction along the reactor axis. It is readily observed that with a decrease in velocity, the difference between the EO mole fraction profile of gas and solid phase increases. This behavior has been attributed to the distinct resistances of kinetically controlled and the mass transfer resistance of gas film around the catalyst pellets.

In fact, higher gas velocities prevent the formation of clear boundaries between gas and solid phases.[17]

5. CONCLUSIONS

In this work a heterogeneous one-dimensional transient model was developed in the presence of long-term deactivation of Ag/Al_2O_3 as catalytic system, considering two different solid and fluid phases along with their corresponding heat and mass exchanges. In order to determine the level of optimum EDC a MLP neural network was used. In addition, the effect of inlet gas velocity on the similarity of gas and solid phases was investigated. The results are as follows:

1. The results of steady state simulation showed that the behavior of the gas phase is obviously different from that of the corresponding catalyst phase under the same operating conditions. Also, the obtained results were used as the initial values for the dynamic heterogeneous model.
2. There was a good agreement between simulation results of the dynamic model and historical process data of the plant over 1100 days. The error of simulation was found to be less than 5%.
3. Results of the ANN modeling showed that the maximum selectivity occurs in the range of 0.37−0.42 ppm of EDC.
4. It was observed that with decrease of velocity the difference between the EO mole fraction of gas and solid phase increases. This behavior was attributed to the distinct resistances of kinetically controlled and the mass transfer resistance of gas film around the catalyst pellets.

AUTHOR INFORMATION

Corresponding Author

*To whom Correspondence should be addressed. Tel.: +98 711 2303071; Fax: +98 711 6287294. E-mail address: rahimpor@shirazu.ac.ir (M. R. Rahimpour).

NOMENCLATURE

A_c = cross section area of each tube (m^2)
A_i = inner area of each tube (m^2)
A_o = outside are of each tube (m^2)
a = activity of catalyst
a_v = specific surface area of catalyst pellet ($m^2\ m^{-3}$)
C_{P_g} = specific heat of the gas at constant pressure ($J\ mol^{-1}$)
C_{P_s} = specific heat of the solid at constant pressure ($J\ mol^{-1}$)
C_t = total concentration ($mol\ m^{-3}$)
D_i = tube inside diameter (m)
D_{ij} = binary diffusion coefficient of component i in j ($m^2\ s^{-1}$)
D'_m = diffusion coefficient of component i in the mixture ($m^2\ s^{-1}$)
D_o = tube outside diameter (m)
D_p = particle diameter (m)
E_d = activation energy used in the deactivation model ($J\ mol^{-1}$)
F_t = total molar flow per tube ($mol\ s^{-1}$)
f_i = partial fugacity of component i (bar)
$\Delta H_{f,i}$ = enthalpy of formation of component i ($J\ mol^{-1}$)
ΔH_{298} = enthalpy of reaction at 298 K ($J\ mol^{-1}$)
h_f = gas−solid heat transfer coefficient($W\ m^{-2}\ K^{-1}$)
h_i = heat transfer coefficient between fluid phase and reactor wall ($W\ m^{-2}\ K^{-1}$)
h_o = heat transfer coefficient between coolant stream and reactor wall ($W\ m^{-2}\ K^{-1}$)
K = conductivity of fluid phase ($W\ m\ K^{-1}$)
K_d = deactivation model parameter constant (s^{-1})
K_{gi} = mass transfer coefficient for component i ($m\ s^{-1}$)
L = length of reactor (m)
M_i = molecular weight of component i ($g\ mol^{-1}$)
N = number of components used in the model ($N = 5$)
P = total pressure (bar)
R = universal gas constant ($J\ mol^{-1}\ K^{-1}$)
R_p = particle radius (m)
T = bulk gas phase temperature (K)
T_s = temperature of solid phase (K)
T_{shell} = temperature of coolant stream (K)
t = time (s)
U_{shell} = overall heat transfer coefficient between coolant and process streams ($W\ m^{-2}\ K^{-1}$)
U = superficial velocity of fluid phase ($m\ s^{-1}$)
u_g = linear velocity of fluid phase ($m\ s^{-1}$)
y_i = mole fraction of component i in the fluid phase ($mol\ mol^{-1}$)
y_{is} = mole fraction of component i in the solid phase ($mol\ mol^{-1}$)
z = axial reactor coordinate (m)

Greek Letters

ε_B = void fraction of catalytic bed ($m^3\ m^{-3}$)
ρ_B = density of catalytic bed ($kg\ m^{-3}$)
ρ_g = density of fluid phase($kg\ m^{-3}$)
ρ_s = density of solid phase($kg\ m^{-3}$)

Abbreviations

ANN = artificial neural network
DAEs = differential algebraic equations
EDC = ethylene dichloride

EO = ethylene oxide
GPLE = general power law equation
MLP = multilayer perceptron
ODEs = ordinary differential equations

REFERENCES

(1) Young-Chul, K.; Nam-Cook, P.; Jae-Soon, S.; Sang Ryang, L.; Yong Jun, L.; Dong, J. M. Partial oxidation of ethylene to ethylene oxide over nanosized Ag/α-Al2O3 catalysts. *Catal. Today* **2003**, *87*, 153–162.

(2) Zhou, X.-G.; Yuan, W. K. Optimization of fixed-bed reactor for ethylene epoxidation. *Chem. Eng. Proc.* **2005**, *44*, 1098–1107.

(3) Siriphong, R.; Sumaeth, C.; Johannes, W. S.; Vissanu, M. Catalytic activity of ethylene oxidation over Au, Ag and Au−Ag catalysts: Support effect. *Catal. Commun.* **2007**, *8*, 57–64.

(4) Michael, S.; Stavros, P. Ethylene oxidation on silver catalysts: Effect of ethylene oxide and of external transfer limitations. *Chem. Eng. Commun.* **1986**, *44*, 53–74.

(5) Borman, P. C.; Westerterp, K. R. An experimental study of the kinetics of the selective oxidation of ethene over silver on α-alumina catalyst. *Ind. Eng. Chem. Res.* **1995**, *34*, 49–58.

(6) Gianpiero, G.; Tronconi, E. Simulation of structured catalytic reactors with enhanced thermal conductivity for selective oxidation reactions. *Catal. Today* **2001**, *69*, 63–73.

(7) Van Santen, R. A.; Kuipers, P. C. E. Mechanism of ethylene epoxidation. *Adv. Catal.* **1987**, *35*, 265–270.

(8) Boskovic, G.; Wolf, D.; Brückner, A.; Baerns, M. Deactivation of a commercial catalyst in the epoxidation of ethylene to ethylene oxide-basis for accelerated testing. *J. of Cata.* **2004**, *224*, 187–196.

(9) Vasco de Toledo, E. C.; de Santana, P. L.; Wolf Maciel, M. R.; Filho, R. M. Transient modeling of a three-phase catalytic slurry reactor. *Chem. Eng. Sci.* **2001**, *56*, 6055.

(10) Setinca, L. J. Transients of a mixed slurry reactor for the three phase methanol synthesis. *Chem. Eng. Sci.* **2001**, *56*, 1608.

(11) Quinta Ferreira, R.; Almeida Costa, C.; Masetti, S. Reverse reactor for a selective oxidation process. *Chem. Eng. Scie.* **1999**, *54*, 4615–4627.

(12) Hwang, S.; Smith, R. Heterogeneous catalytic reactor design with optimum temperature profile I: application of catalyst dilution and side-stream distribution. *Chem. Eng. Sci.* **2004**, *59*, 4229–4243.

(13) Hwang, S.; Smith, R. Heterogeneous catalytic reactor design with optimum temperature profile II: application of non-uniform catalyst. *Chem. Eng. Sci.* **2004**, *59*, 4229–4243.

(14) Cornelio Avi. A. Dynamic Modelling of an Industrial Ethylene Oxide Reactor. *Ind. Chem. Eng. Sect. A* **2006**, *48*, No.3.

(15) Aryana S.; Ahmadi M.; Gomes V.; Romagnoli J.; Ngian K. Modeling and optimization of an industrial ethylene oxide reactor. *Chem. Prod. Proc. Model.* **2009**, *4*, Article 14.

(16) Lahiri, S. K.; Khalfe, N. Process modeling and optimization of industrial ethylene oxide reactor by integrating support vector regression and genetic algorithm. *Can. J. Chem. Eng.* **2009**, *87*, 118–128.

(17) Rezaie, N.; Jahanmiri, A.; Moghtaderi, B.; Rahimpour, M. R. A comparison of homogeneous and heterogeneous dynamic models for industrial methanol reactors in the presence of catalyst deactivation. *Chem. Eng. Proc.* **2005**, *44*, 911–21.

(18) Rahimpour, M. R.; Fathikalajahi, J.; Jahanmiri, A. Selective kinetic deactivation model for methanol synthesis from simultaneous reaction of CO_2 and CO with H_2 on a commercial copper/zinc oxide catalyst. *Can. J. Chem. Eng.* **1998**, *76*, 1–9.

(19) Rahimpour, M. R.; Satar, S.; Baniadam, M.; Fathikalajahi, J. Incorporation of flexibility in design of methanol synthesis reactor. *Chem. Eng. Technol.* **2003**, *26* (6), 672–8.

(20) Rahimpour, M. R.; Moghtaderi, B.; Jahanmiri, A.; Rezaie, N. Operability of an industrial methanol synthesis reactor with mixtures of fresh and partially deactivated catalyst. *Chem. Eng. Technol.* **2005**, *28* (2), 226–34.

(21) Velardi, S. A.; Barresi, A. Methanol synthesis in a forcedunsteadystate reactor network. *Chem. Eng. Sci.* **2002**, *57* (15), 2995–3004.

(22) Khademi, M. H.; Jahanmiri, A.; Rahimpour, M. R. A novel configuration for hydrogen production from coupling of methanol and benzene synthesis in a hydrogenpermselective membrane reactor. *Int. J. Hydrogen Energy* **2009**, *34* (12), 5091–5107.

(23) Domestic Petrochemical Complex; Operating data sheets of ethylene oxide plant, 2004−2007.

(24) Rahimpour, M. R.; Elekaei, H. Optimization of a novel combination of fixed and fluidized-bed hydrogen-permselective membrane reactors for Fischer−Tropsch synthesis in GTL technology. *Chem. Eng. J.* **2009**, *152* (2−3), 543–555.

(25) Khademi M. H.; Setoodeh P.; Rahimpour M. R.; Jahanmiri A. Optimization of methanol synthesis and cyclohexane dehydrogenation in a thermally coupled reactor using differential evolution (DE) method. **2009**, *34*(16), 6930−6944.

(26) Papavassiliou, V.; Wagner, M. L. Ballast gas for heat transfer control in fixed-bed reactors. *Chem. Eng. Sci.* **1999**, *54*, 3683–3689.

(27) Froment, G. F.; Bischoff, K. B. *Chemical Reactor Analysis and Design*; Wiley: New York, 1990.

(28) Rahimpour, M. R.; Asgari, A. Production of hydrogen from purge gases of ammonia plants in a catalytic hydrogen-perm selective membrane reactor. *Int. J. Hydrogen Energy* **2009**, *34* (14), 5795–5802.

(29) Cussler, E. L.; Diffusion, *Mass Transfer in Fluid Systems*; Cambridge University Press, 1997.

(30) Baehr, H. D.; Stephan, K. *Heat and Mass Transfer*; Springer-Verlag: Berlin, 2006.

(31) Poling Bruce, E.; Prausnitz John, M.; O'Connell John, P. *The Properties of Gases and Liquids*, 5th ed.; McGraw-Hill: New York, 2004.

(32) Reid, R. C.; Sherwood, T. K. Prausnitz, J. *The Properties of Gases and Liquids*, 3rd ed.; McGraw-Hill: New York, 1987.

(33) Albert Vannice, M. *Kinetics of Catalytic Reactions*: Springer, 2005.

(34) Holman, J. P. *Heat Transfer*; McGraw-Hill: New York, 2001.

(35) Stegelmann, C.; Schiødt, N. C.; Campbell, C. T.; Stoltze, P. Microkinetic modeling of ethylene oxidation over silver. *J. Catal.* **2004**, *221*, 630–649.

(36) Gu, Y. L.; Gao, Z.; Jin, J. Q. Kinetic models for ethylene oxidation to ethylene oxide. *Petrochem. Technol.* **2003**, *32* (Suppl), 838–840.

(37) Bartholomew, C. H. Mechanisms of catalyst deactivation. *Appl. Catal. A: Gen.* **2001**, *212*, 17–60.

(38) Shampine, L. F.; Gladwell, I. Thompson, S. Solving ODEs with MATLAB; Cambridge University: New York, 2003.

(39) Kordabadi, H.; Jahanmiri, A. Optimization of methanol synthesis reactor using genetic algorithms. *Chem. Eng. J.* **2005**, *108*, 249–255.

(40) Kordabadi, H.; Jahanmiri, A. A pseudo-dynamic optimization of a dual-stage methanol synthesis reactor in the face of catalyst deactivation. *Chem. Eng. Process.: Process Intensif.* **2007**, *46* (12), 1299–1309.

(41) Rahimpour, M. R.; Lotfinejad, M. Enhancement of methanol production in a membrane dual-type reactor. *Chem. Eng. Technol.* **2007**, *30*, 1062–76.

(42) Rahimpour, M. R.; Lotfinejad, M. Co-current and counter-current configurations for a membrane dual-type methanol reactor. *Chem. Eng. Technol.* **2008**, *31* (1), 38–57.

(43) Rahimpour, M. R.; Lotfinejad, M. A comparison of auto-thermal and conventional methanol synthesis reactor in the presence of catalyst deactivation. *Chem. Eng. Proc.* **2008**, *47* (12), 2121–30.

(44) Rahimpour, M. R.; Lotfinejad, M. A comparison of co-current and counter-current modes of operation for a dual-type industrial methanol reactor. *Chem. Eng. Proc.* **2008**, *47* (9−10), 1819–30.